Journal of Photochemistry and Photobiology A: Chemistry 332 (2017) 306–315

Contents lists available at ScienceDirect

Journal of Photochemistry and Photobiology A: Chemistry

journal homepage: www.elsevier.com/locate/jphotochem

Synthesis, photophysical properties and spectroelectrochemical characterization of 10-(4-methyl-bipyridyl)-5,15-(pentafluorophenyl) corrole☆

Rhannanda C. Pivetta[a], Bruna L. Auras[a], Bernardo de Souza[a], Ademir Neves[a], Fábio S. Nunes[b], Leandro H.Z. Cocca[c], Leonardo De Boni[c], Bernardo A. Iglesias[d,*]

[a] Laboratório de Bioinorgânica e Cristalografia (LABINC), Departamento de Química, Universidade Federal de Santa Catarina, 88040-900, Florianópolis, SC, Brazil
[b] Departamento de Química, Universidade Federal Do Paraná, Cx. Postal 19081, 81531-980 Curitiba, PR, Brazil
[c] Instituto de Física de São Carlos, Universidade de São Paulo, CP 369, 13560-970 São Carlos, SP, Brazil
[d] Departamento de Química, Universidade Federal de Santa Maria – UFSM, 97105-900 Santa Maria, RS, Brazil

ARTICLE INFO

Article history:
Received 29 June 2016
Received in revised form 15 August 2016
Accepted 10 September 2016
Available online 11 September 2016

Keywords:
Corroles
Trans-A_2B corroles
Photophysical properties
Photodynamic therapy PDT

ABSTRACT

The new bipyridyl-corrole dye 10-(4-methyl-bipyridyl)-5,15-(pentafluorophenyl)corrole, encompassing a coordenative methyl-bipyridine moiety (corrole **2**), was prepared starting from 5-(pentafluorophenyl) dipyrromethane and reacting it with methyl-bipyridyl-carboxaldehyde by Gryko's methodology. It was further characterized by spectroscopic and electrochemical methods. In addition, we investigated experimental photophysical properties, photostability, reactive oxygen species generation (ROS) and aggregation phenomena, which are relevant when selecting photosensitizers used in photodynamic therapy and many other applications. Photophysical properties have demonstrated that the corrole **2** dissolved in dichloromethane has a triplet quantum yield formation of about 51%. Fluorescence and internal conversion quantum yields of 4% and 45%, respectively, have also been determined in order to evaluate which could be was the main pathway of the excited state relaxation. Triplet state formation was also confirmed by measuring indirectly $^1O_2$ generation. Additionally, quantum chemistry calculations indicated that the most probable intersystem-crossing pathway takes place through S_1-T_1, corroborating our rate equation model.

© 2016 Elsevier B.V. All rights reserved.

1. Introduction

Corroles are tetrapyrrolic macrocycle, 18 π-electron Hückel aromatic compounds closely related to porphyrin with a direct pyrrole–pyrrole linkage lacking one methine bridge [1]. Description of the first method of corrole synthesis method was carried out by Johnson and Kay [2] in the late 1960s, motivated by the similarity of corroles to that of cobalt chelating corrin in vitamin B_{12}. A one-pot synthesis described by Gross and collaborators [3] in the 90's followed by remarkable development in the synthesis of corroles, revolutionized the understanding of this unique tetrapyrrolic derivative.

With respect to their physico-chemical properties, corroles show relatively higher fluorescence quantum yields and molar absorptivities than the corresponding porphyrin macrocycles [4]. Moreover, the non-innocent nature of the corrole ligand in many coordination complexes is now well documented [5]. Their trianionic nature due to three inner nitrogen protons results in intriguing properties to corroles, which are significantly different from those of porphyrin macrocycles. In particular, the ability to stabilize relatively higher oxidation states of metals than those of the corresponding porphyrin complexes has increased the use of metallocorroles in catalytical processes [6]. During the last years, corroles have demonstrated potential applications in the field of photochemical sensors [7], artificial photosynthesis [8], material chemistry [9] and nano-biomedical applications [10].

Free-base corroles usually present lower stability under light and air than the porphyrin macrocycles [11]. This mainly originates

☆ The authors state that the revised article "*Synthesis, photophysical properties and spectroelectrochemical characterization of 10-(4-methyl-bipyridyl)-5,15-(pentafluorophenyl)corrole*" is original and unpublished and is not being considered for publication elsewhere.

* Corresponding author.
E-mail address: bernardopgq@gmail.com (B.A. Iglesias).

http://dx.doi.org/10.1016/j.jphotochem.2016.09.008
1010-6030/© 2016 Elsevier B.V. All rights reserved.

from the electron-rich nature of corrole, reduced aromaticity and deformation of the macrocycles from planarity due to steric hindrance at the core. However, the tri-(pentafluorophenyl)-substituted corrole has been identified to be stable under oxidative degradation when in light and air due to the presence of electron withdrawing pentafluorophenyl groups at the *meso*-carbon and probably is a good choice when higher stability is desired. A few successful functionalizations of corroles reported in the literature shows significant effect on the electronic properties of the corrole macrocycle [12]. Functionalization of the aryl ring at the *meso*-position or in the *para*-position with a pentafluorophenyl is the most common and relatively easy modification [13]. Insertion of strategic aldehydes in this type of compounds, which contains coordinating groups such as pyridines [14] or bipyridines [15], can add new properties, thereby granting new possibilities into the corrole chemistry.

Therefore, partially inspired by the lack of literature reports on peripheral functionalization with coordinating ligands at the *meso*-carbon position of corrole, we report the successful direct 4-Mebpy-corrole conjugates (corrole **2**) obtained by cyclization between C_6F_5-dipyrromethane with 4-(methylbipyridyl)-carboxaldehyde moiety.

The structure and electronic properties of this corrole derivative were investigated along with their eletroctrochemical/spectroelectrochemical properties. In addition, we have performed a preliminary study of their photophysical properties, determining fluorescence, internal conversion and intersystem-crossing quantum yields. All these parameters were determined by employing Time-resolved fluorescence and Pulse Train Fluorescence (PTF) techniques. Furthermore, the most probable intersystem-crossing pathway, which occurs through S_1-T_1 transition, was also indicated by quantum chemistry calculations of spin-orbit coupling matrix elements using a CASSCF wavefunction. The present work indirectly explored the potential use of this chemically modified bipyridyl-corrole to be used in photodynamic therapy (PDT) studies.

2. Experimental

2.1. Materials

All reagents were of analytical grade and were purchased from Aldrich or national suppliers. Column chromatography was carried out using silica-flash 230–400 mesh from Aldrich. Analytical preparative thin-layer chromatography was performed on aluminum sheets (1.0 mm thick) Merck TLC silica-gel 60 F_{254}.

2.2. Physical measurements

Corrole analysis in a high resolution ESI-MS. (HRMS-ESI) was performed on a micrOTOF QII mass spectrometer (Bruker Daltonics, Billerica, MA). Mass spectra were performed with a methanolic solutions of concentration around 500 ppb with a flow of 180 μL/min and at capillary of 3000 V–4500 V ^{1}H, ^{13}C, ^{19}F and COSY 2D NMR spectra were recorded with a Bruker Avance III spectrometer at 600.13 (^{1}H), 150.9 (^{13}C) and 564.68 MHz (^{19}F) respectively. $CDCl_3$ was used as solvent and TMS as the internal reference. The chemical shifts are expressed in δ (ppm) and coupling constants (*J*) are given in Hertz (Hz). The UV–vis absorption spectra were measured in the 1.0 mm optical path length of a quartz cuvette using a SHIMADSZU UV-1800, with a concentration of about 50 μM in dichloromethane solution. Fluorescence spectra and fluorescence quantum yields were measured in the 1.0 cm optical path length of a quartz cuvette using a HITACHI F7000 fluorimeter with a concentration 50 times lower than the one used to measure the absorption. It was diluted to minimize re-absorption by the compound.

Cyclic voltammetry was carried out with an IVIUM CompactStat potentiostat/galvanostat. A gold disc electrode was employed in the measurements at 0.1 mol/L $TBAPF_6$ (tetrabutylammonium hexafluorophosphate as support electrolyte). $Ag/AgNO_3$ electrode ($[Ag^+]$ = 0.01 mol/L in MeCN solution of $TBAPF_6$ 0.1 mol/L) was used as reference (0.503 V *versus* SHE) and platinum wire was employed as auxiliary electrodes, respectively. Typical experiments were conducted with a mM concentration in dichloromethane solutions at room temperature. Spectroelectrochemistry measurements were performed with the IVIUM CompactStat potentiostat/galvanostat attached an Agilent 8453 diode-array spectrophotometer with about ≈1 mmol/L complex and 0.1 mol/L of $TBAPF_6$ acetonitrile solutions. A three electrode system was used with a thin layer cell of 0.1 cm of internal optical path length. A platinum minigrid was used as transparent working electrode, in the presence of a small $Ag/AgNO_3$ reference electrode and a platinum auxiliary electrode. The compounds 2-(4-methylpyridin-2-yl) pyridine-4-carbaldehyde **1** and 2,3,4,5,6-(pentafluorophenyl) dipyrromethane [16] were synthesized according to the literature.

2.3. Pulse train fluorescence technique

The experimental setup used to measure intersystem crossing rate of corrole **2** includes a frequency-doubled (532 nm), mode-locked and Q-Switched Nd:YAG laser. This laser system delivers a sequence of about 30 short pulses (100 ps FWHM) modulated by the Q-switched envelope (pulse train). The pulses in the train are separated approximately 13.2 ns. The laser characteristic output profile is shown in the Supplementary information section (ESI†, Section 6) with a repetition rate that can be chosen from 3 up to 800 Hz. In the present work, the repetition rate was set at 300 Hz, which delivered an output power of about 30 mW for the whole pulse train [17].

2.4. Electronic structure calculations

All calculations were performed by using the software ORCA, with default parameters unless stated otherwise [18]. The geometry for the corrole **2** and its other three tautomers were first optimized with DFT up to an energy change of less than 5.0×10^{-6} hartree, using the GGA functional PBE [19] and the triple zeta valence basis Def2-TZVP(-F) [20] at the potential of the solvent (dichloromethane), by using the COSMO approach [21]. To obtain a better long range interaction description, the atom-pairwise dispersion correction by Grimme with Becke-Johnson damping was also added [22]. The resolution of identity (RI) for the four center integrals was employed with the corresponding auxiliary basis. After geometry optimization, the frequencies for the normal modes were obtained and no negative energies were found, confirming that the structures were indeed a minimum. A TD-DFT calculation with COSMO corrections was performed to obtain the excited state wave functions and the transition oscillator strengths without TDA approximation [23] and using the same basis. In this part, we searched for the first 25 roots.

The spin-orbit coupling constants for **2** and the equivalent hydrogen substituted molecule were obtained from state-averaged CASSCF wave functions with energies corrected with NEVPT2, choosing a small active space of six electrons in six π-molecular orbitals (CAS(6,6)). Before the perturbation treatment, each averaged state had the orbitals relaxed by one step, as described on ORCA manual (option nev_canonstep = 3). In order to reduce the complexity of the problem, we have chosen the smaller Def2-SV(P) basis functions, also using COSMO to simulate solvent effects. The spin-orbit matrix elements were calculated by using the complete

mean-field approach to the Breit-Pauli operator, including one electron terms, computing the Coulomb contribution with RI, calculating the Exchange contribution *via* exact one center integrals (including spin-other orbit interaction) and also including local DFT correlation (SOCFlags 1,3,3,1 in the SOC module of ORCA) [18].

2.5. $^1O_2$ generation and photostability assays

In a typical experiment of 1.3-diphenylisobenzofuran (DPBF) photodegradation [24], 2.0 mL of 100 μM DPBF in DMSO was mixed with 0.4 mL (50 μM) of corrole **2**. The flask was completed with DMSO until a final volume of 4.0 mL. In order to measure $^1O_2$ generation, absorption spectra of the solutions (samples and standard) were recorded for different exposure times by using a 660 nm diode laser positioned 1.0 cm from the sample (TheraLase DMC, São Carlos, SP, Brazil) with an average power of 100 mW. The singlet oxygen production quantum yield (Φ_Δ) was calculated by using Eq. (1):

$$\Phi_\Delta = \frac{\Phi_\Delta^{std} k}{k^{std}} \cdot {}^{I^{std}}\Big/_{I} \quad (1)$$

in which, $I^{std}/I = \left(1 - 10^{A_{std}}\right)/\left(1 - 10^{A}\right)$, Φ_Δ^{std} is the singlet oxygen quantum yield of standard sample (in our case, Zinc Phthalocyanine (ZnPc) dissolved in DMSO, $\Phi_\Delta^{std} = 0.67$ [25]), k and k^{std} are the photodegradation kinetic constants for corrole **2** and ZnPc (standard), respectively, and A_{std} and A are the absorbances for ZnPc and corrole **2**, respectively. The photostability of corrole **2** was also monitored by absorption measurements for different exposure times with the same pump diode laser with 100 mW of average power. All experiments were performed in duplicate and independently.

2.6. Aggregation study

The self-aggregation of porphyrin macrocycles is a natural tendency due to the strong attractive interactions between π-systems of the polyaromatic compounds [26]. It is already known that the aggregation degree increases with concentration. In order to investigate possible aggregation of corrole **2**, UV–vis spectra were measured as a function of the concentration using dichloromethane as solvent. Changes in the λ_{max} from the bands in UV–vis spectra were monitored.

2.7. Synthesis of 10-(4-methyl-bipyridyl)-bis-5,10-(pentafluorophenyl)corrole (2)

5-(pentafluorophenyl)dipyrromethane (0.319 g; 1.025 mmol) and the aldehyde **1** (0.108 g; 0.55 mmol) were dissolved in 50 mL MeOH. Subsequently, a solution of HCl_{aq} (37%; 2.5 mL) in H_2O (50 mL) was added and the reaction was stirred at room temperature for 1.5 h. The mixture was extracted with $CHCl_3$, and the organic layer was washed twice with H_2O, dried (Na_2SO_4), filtered, and diluted to 250 mL with $CHCl_3$. A solution of DDQ (0.231 g; 1.025 mmols) in toluene/dichloromethane mixture (1:3; 8 mL) was added, and the mixture was stirred for 20 min. The reaction mixture was concentrated to half of this volume and it was purified first on a silica-gel chromatography column (DCM/*n*-hexane, 1:2, v/v). Then, the resulting residue was purified by preparative silica-gel TLC plates using a mixture of DCM/MeOH (95:5, v/v) to obtain pure dark greenish corrole **2**.

Spectroscopic data for corrole 2: Yield 0.079 g; 0.098 mmol (17%). M.p. > 300 °C (decomp.). ^{1}H NMR (600 MHz, $CDCl_3$): δ = −2.87 (bs, 3H, inner NH), 2.54 (s, 3H, CH_3), 7.19 (d, 1H, J = 6.6 Hz, *m*-Mebpy), 8.11 (d, 1H, J = 5.4 Hz, *m*-bpy), 8.49 (d, 1H, J = 7.2 Hz, *o*-Mebpy), 8.52 (s, 1H, *m*-Mebpy), 8.58 (d, 2H, J = 5.4 Hz, β-H 7,9), 8.72 (s, 4H, β-H 5), 9.06 (d, 1H, J = 6.6 Hz, *o*-bpy), 9.11 (d, 2H, J = 6.0 Hz, β-H 6,8) and 9.23 (s, 1H, *m*-bpy). ^{19}F NMR ($CDCl_3$, 564.68 MHz): −161.70 to −161.68 (m, 2F, F_{meta}); −152.59 (s, 1F, F_{para}) and −137.73 to −137.90 (dd, 2F, J_1 = 11.28 Hz and J_2 = 62.04 Hz, F_{ortho}). ^{13}C NMR (150.9 MHz, $CDCl_3$): δ = 29.88, 117.58, 122.58, 124.88, 126.17, 127.35, 129.43, 148.02, 148.29 and 149.12. HRMS-ESI $[M]^+$: m/z = 799.1756 (calcd for $C_{42}H_{20}N_6F_{10}$: 799.1663).

3. Results

3.1. Design and synthesis of corrole 2

Trans-A_2B-corroles [16] that present a bipyridyl moiety attached at the 10-position of the corrole was studied. We focused our investigation mainly on the relatively simple bipyridines that present bidentate coordinating groups and can be used as a platform of new peripheral complexes [14,15]. Two pentafluorophenyl units were intended to be introduced at the position 5 and 15 of the macrocycle to warrantee good photo-stability of the corrole core during photophysical characterization. Our strategy was to synthesize a bipyridyl-aldehyde derivative which was transformed into the corresponding corrole through the reaction with 5 (pentafluorophenyl)dipyrromethane.

The reaction to obtain the functionalized bipyridyl-aldehyde was based on the formylation reaction between 4,4′-(dimethyl) bipyridine (1.0 equivalent) and SeO_2 (1.3 equivalents) described by Busche and co-workers [27] (Scheme 1). After 24 h under reflux in dry 1,4-dioxane the functionalized aldehyde **1** was isolated in large scale (around 1–2 g; yield 35%). The access to bipyridyl-substituted corrole **2** was performed, according to Gryko and collaborators [16], and involves the condensation of 5-(pentafluorophenyl) dipyrromethane and the adequate aldehyde **1** in a mixture of $MeOH/H_2O$ (50:50; v/v) using HCl as catalyst (Scheme 1). The reaction mixture was maintained under stirring for 1.5 h at room temperature, and, after the usual work up and chromatographic purification, we were able to isolate corrole **2** in 17% yield.

The structure of the corresponding free-base corrole **2** was confirmed by mass spectrometry, NMR, electrochemistry, TD-DFT calculations, UV–vis and fluorescence spectroscopy and their photophysical properties were evaluated (*vide infra*).

3.2. Mass spectrometry and NMR analysis of corrole 2

Considering the characterization of corrole **2**, its high resolution (HRMS-ESI) mass spectrum (ESI†, Fig. S1) shows only one ion peak at m/z 799 ($[M]^+$), in agreement with the *meso*-mono(4-methyl-bipyridyl)-substituted corrole **2**. When the ESI-MS/MS fragmentation processes of **2** are analyzed, we observed a systematic HF loss in the pentafluorophenyl group (ESI†, Fig. S2). In general, the ^{1}H NMR spectrum of corrole **2** showed the expected profile for *trans*-A_2B-corroles molecules. For instance, the signals at δ 9.11, 8.72 and 8.58 ppm correspond to the resonances of the β-pyrrolic protons H-6,8, H-5 and H-7,9 respectively. As expected, the singlet at δ 8.52 ppm and doublets at δ 8.49 and 7.19 ppm with coupling constants (J) of 6.6 and 7.2 Hz were identified as the resonances of the *ortho* and *meta* Me-bpy protons. The signals due to the *meta* and *ortho* protons of the bipyridyl ring between corrole macrocycle and Me-bpy fragment appear at δ 9.23, 9.06 and 8.11 ppm, respectively. The signal corresponding to the inner protons of corrole **2** appear at δ −2.87 and the CH_3 protons (singlet) at δ 2.54, respectively (ESI†, Fig. S3).

The ^{19}F NMR spectrum of compound **2** showed a similar profile as that of 5,10,15-tris(pentafluorophenyl)corroles. For example, the corrole **2** ^{19}F NMR spectrum shows the resonances of the fluorine

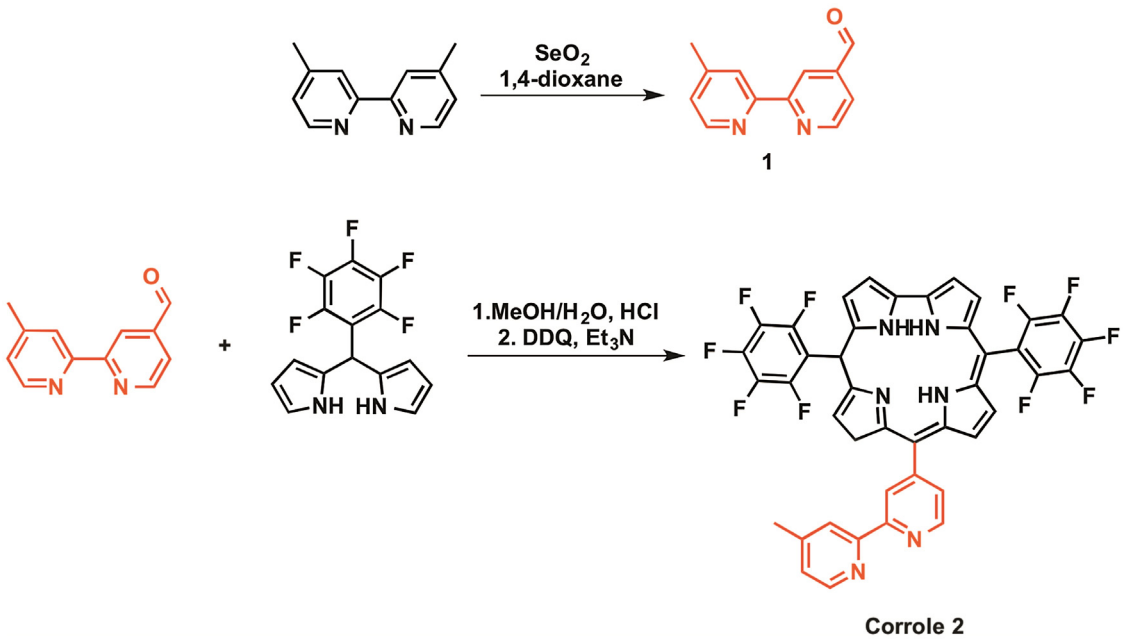

Scheme 1. Synthesis of the functionalized aldehyde **1** and corrole **2**.

atoms in the *meta* position as a multiplet between δ −161.70 and −161.68 ppm, the resonances of *para* atoms appear as a singlet at δ −152.59 ppm and those belonging to *ortho* atoms as double-doublets in the δ −137.73 to −137.90 ppm range (ESI†, Fig. S4). ^{13}C and COSY 2D NMR spectra are found in the Supplementary information Section (see ESI†, Figs. S5 and S6).

3.3. Photophysical properties of corrole 2

Molar absorptivity (**solid line**) and steady-state emission spectra (**dashed line**) of corrole **2** dissolved in dichloromethane (DCM) are presented in Fig. 1. The UV–vis spectrum contains a strong Soret absorption band in the 400–450 nm range with a maximum magnitude of about 2.1×10^5 L/mol cm. Weaker bands, which a maximum molar absorptivity of about ten times lower than the Soret band, between 500 and 700 nm, were attributed to the Q bands. It is possible to see that the shape of the spectrum is a single emission band that ends at approximately 750 nm.

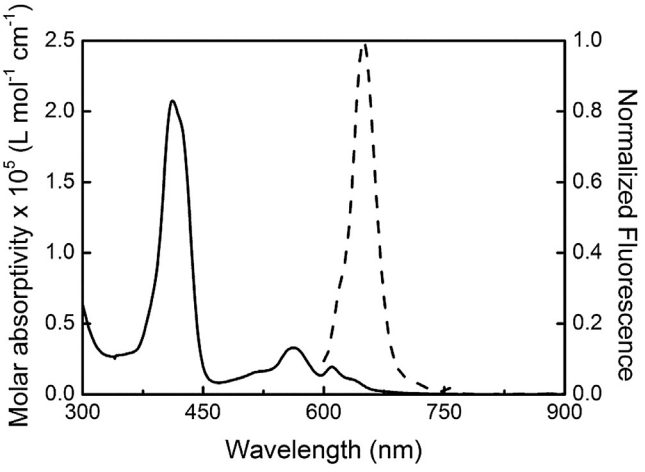

Fig. 1. UV–vis (solid line) and fluorescence (dashed line) spectra of corrole **2** dissolved in dichloromethane.

The fluorescence quantum yield (ϕ_f) [28] for corrole **2** dissolved in dichloromethane was measured using the well known method described by Brouwer and collaborators [29], in which a sample with a known ϕ_f is used as reference to calibrate and determine the fluorescence quantum yields of unknown samples. In our case, we used Hematoporphyrin dissolved in DMSO as reference sample with ϕ_f^{ref} of about 0.08 [30] in a low concentration to avoid aggregation. In order to avoid re-absorption of the emission by the samples, the optical densities were chosen to be around 0.1 for a square quartz cuvette of 1.0 cm optical path length. Therefore, the fluorescence spectra of the reference and samples were measured by exciting both at the same wavelengths. We used four different wavelengths, 420, 500, 535 and finally 570 nm, to determine the ϕ_f of corrole **2**. Once fluorescence spectra were recorded for both samples, fluorescence quantum yields of the samples were obtained by using Eq. (2):

$$\phi_f = \phi_f^{ref} x \frac{\int_{\lambda_0}^{\lambda_f} F(\lambda) d\lambda}{\int_{\lambda_0}^{\lambda_f} F_{ref}(\lambda) d\lambda} x \frac{f_{ref}}{f} x \frac{n^2}{n_{ref}^2} \quad (2)$$

in which, f is the absorption factor, which is defined, as the ratio of the absorbed to the incident light $f = 1 - 10^{-A(\lambda_{ex})}$, such that $A(\lambda_{ex})$ is the absorbance of the sample at the excitation wavelength. $F(\lambda)$ is the fluorescence spectrum as a function of the wavelength, integrated in a wavelength range that the full spectrum contemplates n is the refractive index (1.424, DCM) and n_f is the reference refractive index (1.4793, DMSO) [31]. The obtained fluorescence quantum yield is around 4% for all wavelengths mentioned. This value is in the same order of magnitude to those observed for other corrole derivatives dissolved in DCM [32,33].

The next step of our photophysical characterization was to evaluate the fluorescence lifetime (τ_f). This time can be obtained through time resolved fluorescence measurement (see description on ESI†). In Fig. 2, it is possible to observe the fluorescence decay (**symbols**) as a function of the time. To fit this curve (**solid line**), we used a mono-exponential function ($I(t) = I_0 e^{-t/\tau_f}$), which properly describes well the experimental points obtained within the

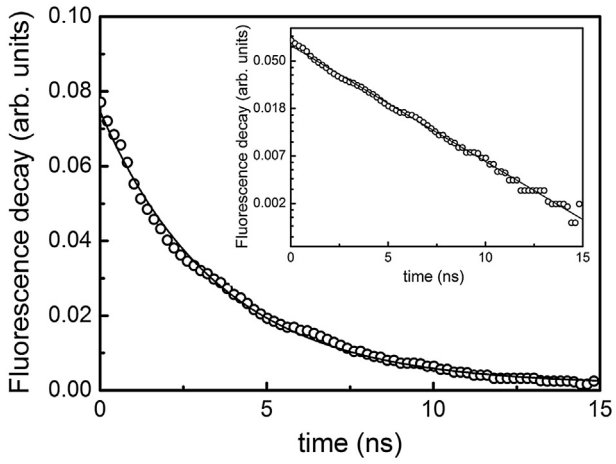

Fig. 2. Fluorescence decay of the corrole **2**. The solid line represents the best single exponential fit. The inset shows the linearization of the experimental fluorescence decay, and the solid line is the best linear fit to the experimental points.

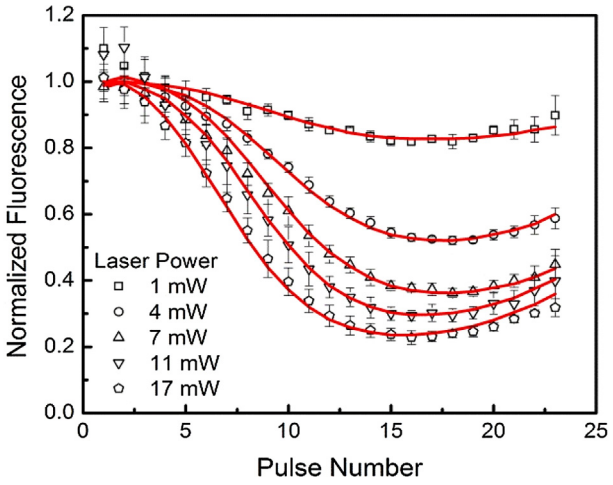

Fig. 4. Normalized fluorescence signal pattern obtained with different laser powers (**symbols**) by the PTF technique as a function of the pulse number of the pulse train. The solid lines represent the best fit obtained using the rate equations model described by Eq. (3).

experimental time resolution range (>700 ps). The best exponential fit to the experimental curve provided a $\tau_f = 3.8 \pm 0.2$ ns. The inset of Fig. 2 depicts the linearization of the fluorescence signal as a function of the time. One can see that this graph presents a single linear behavior, which agrees with a single decay relaxation time.

The fluorescence lifetime measured for corrole **2** is in agreement with those obtained for other corrole derivatives dissolved in DCM [12,32,33]. Once the fluorescence lifetime and quantum yields were determined, we were able to estimate the radiative decay rate $k_r = \phi_f/\tau_f$ for corrole **2** dissolved in DCM. In our case, $k_r = 1.05x10^7 s^{-1}$, which gives a radiative decay time of about 95 ns ($\tau_r = 1/k_r$). It is possible to see that the radiative decay time is very slow when compared with the fluorescence lifetime, indicating that probably for corrole **2** the main relaxation mechanisms are the internal conversion (IC) and/or triplet state formation.

In order to determine the most probable mechanism, by IC relaxation (τ_{nr}) or intersystem crossing (τ_{isc}) processes, we used the Pulse Train Fluorescence (PTF) [17] technique (see description on ESI†, Fig. S7) to measure both parameters as complementary results of our photophysical characterization. This technique, already described in the experimental section and in the ESI†, is simple because it uses a single beam and provides as output results information on how the fluorescence signal behaves when a sequence of laser pulses with a well-know pattern excites the sample. An example, of the possible results of the PTF technique is the fluorescence signal decreases as a function of the pulse number of the pulse train. This effect is observed on the corrole **2** and the results are presented in Fig. 4. In most cases, the depletion of the cumulative fluorescence signal occurs if an intersystem crossing process exists.

Using PTF, the results obtained for corrole **2** can be easily modeled just by using a three rate equation systems, which are able to describe the population dynamics over the evolved electronic states, as illustrated in the Jablonski diagram (Fig. 3). It is not necessary to take in consideration higher excited states (singlets or triplets), because the relaxation of those states occurs in the sub-picosecond regime and does not modify the fluorescence signal of the first excited state. In other words, population in higher excited states will relax during the duration of each 100 ps pulse. It is necessary to know, previously, some of the parameters of the sample such as the absorption cross-section of the ground state (S_0) to the first excited (S_1), (σ_{01}), the fluorescence lifetime (τ_f) and the triplet relaxation time ($\tau_T = 1/k_T$). Once these parameters are obtained with other experimental techniques, such as linear absorption and time-resolved fluorescence, the intersystem crossing rate, $k_{isc} = 1/\tau_{isc}$, can be determined as the unique parameter of adjustment in the rate equation model becomes possible. Modeling the PTF signal and knowing that the fluorescence signal intensity is proportional to the population of the first singlet excited state S_1, the population responsible for the depletion of the fluorescence through decay to the triplet state, can be determined and only depends on τ_{isc}.

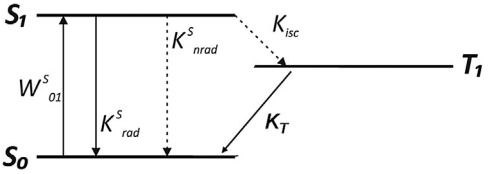

Fig. 3. Jablonski three level diagram, representing ground (S_0), first excited (S_1) singlet states and a triplet excited state (T_1). Radiative and non-radiative transitions are depicted by arrows.

Additionally, the numerical solution to the rate equations requires a boundary condition provided by a population normalization ($\sum n_i(t) = 1$) and stating an initial condition, $n_{S_0}(t) = 1$. Thus, the rate equations corresponding to the system depicted in Fig. 3 can be described by Eq. (3):

$$\frac{dn_{S_0}(t)}{dt} = -W_{01}^s n_{S_0}(t) + (k_f - k_{isc}) n_{S_1}(t) + n_{T_1} k_T;$$

$$\frac{dn_{S_1}(t)}{dt} = +W_{01}^s n_{S_0}(t) - k_f n_{S_1}(t); \quad (3)$$

$$\frac{dn_{T_1}(t)}{dt} = +k_{isc} n_{S_1}(t) - n_{T_1} k_T.$$

From the rate equations, it is possible to notice that changes in the population fractions as a function of time starts with the initial transition probability between the ground and first singlet excited states, $W_{01} = \phi\sigma_{01}$, in which the pulse fluence is defined as $\phi = I/h\nu$, with I as the intensity of each individual pulse of the train. Therefore, when the first train of pulses arrives on the sample, the population of S_0 excited to S_1 is proportional to the

Table 1
Summary of the photophysical data for corrole **2** dissolved in DCM.

Compound	ϕ_F	ϕ_{nr}	ϕ_T	$\tau_{f\,(ns)}$	k_r (10^7 s^{-1})	k_{nr} (10^7 s^{-1})	k_{isc} (10^7 s^{-1})
Corrole **2**	0.04	0.45	0.51	3.8 ± 0.2	1.05	11.94	13.33

intensity of that pulse, to the absorption cross-section, and to the initial population of the ground state ($n_{S_0}(t) = 1$). Subsequently, part of the population in the S_1 can relax to the ground state with a rate defined the sum of the fluorescence and internal conversion rates and can undergo an intersystem crossing mechanism to the triplet state. Once molecules in the T_1 state, they become trapped in this state for a time defined by the triplet state lifetime and do not contribute anymore to the fluorescence signal during the relaxation time of the triplet state.

Continuing the interaction between the sample and the pulse train envelope, after 13.2 ns a second pulse of the train arrives and excites another part of the population. For this pulse, S_0 population is now defined as $n_{S_0} < 1$, since part of the initial population was already on the excited states due to the first pulse. This process will be repeat until the last pulse of the envelope interacts with the sample, giving a cumulative population on the triplet state. Thus, solving numerically the rate equations and using the pulse train envelope as fluence input, the population in each of the three states is determined as a function of the time, including the population responsible of the fluorescence signal.

The data obtained from PTF (**symbols**) and simulated (**solid lines**) by the rate equations are illustrated in Fig. 4 as a function of the pulse train envelope power. In this figure, it is possible to see how the fluorescence signal evolves as a function of the pulse number for each individual laser power. All measurements provided at the beginning of the pulse train had the same value for the Normalized Fluorescence (NF) signal, defined as the ratio of the fluorescence signal to the reference pulse train input intensity. Thus, the NF signal close to unit (pulse number = 1), means that the population transferred to the triplet state is still low and has little influence on the fluorescence signal. However, once the subsequent pulses interact (pulse number > 3), the NF signal presents values lower than one the fluorescence signal is not anymore proportional to the intensity of the respective reference pulse and the population of the triplet state gets larger. After the pulse number 17, one can notice that the fluorescence signal increases with respect to the reference intensity pulse. This behavior can be influenced by the triplet lifetime.

As corrole compounds present triplet lifetime on the scale of hundreds of nanoseconds [33], at the end of the pulse train, the ground state starts to be repopulated by the triplet relaxation, $T_1 \rightarrow S_0$, providing more molecules to be promoted to the first singlet excited state, increasing once more the fluorescence signal. Furthermore, Fig. 4 depicts an increase of the ratio between the fluorescence signal and the reference intensity pattern as a function of the laser power, which is expected to happen as the population transferred to the excited states is proportional to the fluence of the pulse train.

The interesting fact is that all fitted results were made just by changing the input power, and keeping all other input parameters constants. The solid lines (**fittings**) were obtained by using the same $\sigma_{01}(532nm)$, $\tau_f = 3.8$ ns, and $\tau_T = 260 \pm 40ns$, the last one close to those obtained for similar *meso*-corroles [33]. Even though the error in the triplet state lifetime is considerable, it does not influence the intersystem crossing relaxation time determination. The intersystem-crossing relaxation time is much faster, and the drop in the NF signal (between pulses 3 and 13) is only sensible to τ_{isc}. As the unique parameter to be adjusted in order to fit the experimental results, we obtained for corrole **2** a $\tau_{isc} = 7.5 \pm 0.8$ ns, which is in agreement with other values reported in the literature [33]. With this relaxation time ($\tau_{isc} = 1/k_{isc}$), we can obtain the triplet quantum yield (ϕ_T) by using the following expression $\phi_T = (k_{isc}/k_f)$, giving $\phi_T \cong 51\%$ and $k_{isc} = 13.33x10^7 s^{-1}$. To complete the analysis, the non-radiative quantum yield (IC) ($\phi_{nr} = 1 - \phi_f - \phi_{isc}$) and rate ($k_{nr} = k_f - k_r - k_{isc}$) were obtained, resulting in values of ϕ_{nr} of about 45% and $k_{nr} = 11.94x10^7 s^{-1}$.Once the rate was determined, a non-radiative lifetime ($\tau_{nr} = 1/k_{nr}$)of 8.4 ns was obtained. With these values, one can notice that the main mechanisms involved on the deactivation of the first singlet excited state occurs by an IC process and an ISC to a triplet state, at similar rates. According to ref. [33(a)], the presence of halogen atoms could increase the ISC process, as well as ϕ_T, proportionally to the halogen weight as also observed in porphyrins, but that is not significant here (see CASSCF results) [34,35]. One explanation for the high IC is that the electron-withdrawing of the perfluorination of phenyl groups increases the non-planar distortion of the macrocycle, accelerates the rate of decay from $S_1 \rightarrow S_0$, which competes with ISC mechanism [34,35]. A summary of the photophysical data for corrole **2** dissolved in DCM is shown on Table 1.

3.4. Theoretical TD-DFT results

The optimized geometry for the corrole **2** is displayed on Fig. 5, along with ten frontier orbital energies and the HOMO and LUMO isosurfaces. The geometry portrayed is the most stable of the four tautomers and was here calculated to be 1.07 kJ/mol lower in energy, according to the literature results [36]. The bond lengths and angles are typical for similar corroles, with C—N bonds of about 1.37 Å, a strong intramolecular hydrogen bond of 2.07 Å and a distorted aromatic ring, with a maximum dihedral angle between pyrrole units of 76.2° [36]. Both the HOMO and LUMO are π-molecular orbitals centered on the central ring, with a bandgap of 1.53 eV.

To characterize the transitions observed in the UV–vis spectrum of this molecule, Time Dependent Density Functional Theory (TD-DFT) was employed and vertical excitation energies and oscillator strengths were calculated (ESI†, Fig. S8). From the first twenty-five roots, the simulated UV–vis spectrum with approximately 0.15 eV broad gaussian lineshapes is compared to the experimental in

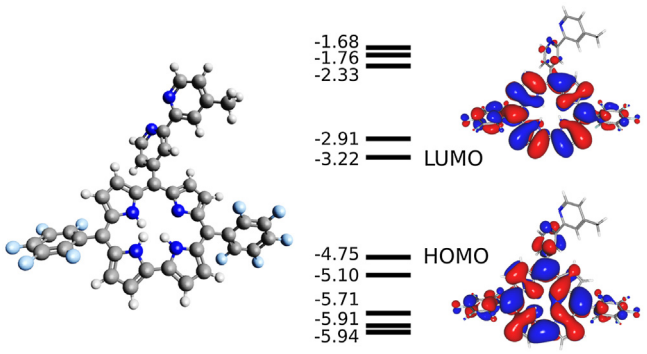

Fig. 5. Optimized geometry of corrole **2**, with ten frontier orbitals with corresponding energies in eV and HOMO and LUMO isosurfaces within 90% probability.

dichloromethane (ESI†, Fig. S9). With the calculated absorption spectrum, a better description of the transitions involved could be obtained and the principal components of each excited state were evaluated. The lower energy region, from 500 to 650 nm, have absorption peaks that correspond to transitions from the corrole π system to the π* molecular orbitals of both the tetrapyrrolic ring and bipyridine, and, at 416 nm, there are transitions from the HOMO to the π* molecular orbitals of the bipyridine and fluorophenyl groups. Those are commonly assigned as the S_0-S_1 and S_0-S_2 transitions, respectively [37]. The orbital picture suggesting an electron jump from the HOMO of corrole **2** to the bipyrine is of particular importance, for it demonstrates the possibility of excited state electron transfer in a possible bimetallic complex involving the central ring and a peripheral metal.

In order to investigate the possibility of intersystem crossing in corrole **2** and possible spin-orbit effects related to fluorine substitution, the spin-orbit coupling matrix elements between some states were calculated using approximations to the Breit-Pauli operator on a SA-CASSCF(6,6) wavefunction with energies corrected by the NEVPT2 perturbation theory [38]. The SA-CASCI was composed of five singlets and three triplets that we found to be sufficient to describe the first excited states and compute the interstate matrix elements. The transition energies obtained were similar to those calculated from TD-DFT, with the first four transition wavelengths being 564, 538, 383 and 363 nm, demonstrating that the rather small active space still can represent the electronic wave function of this system relatively well. The spin-orbit matrix elements of an analog of corrole **2,** in which the fluorine atoms where substituted by hydrogen were also calculated in order to confirm that fluorine substituent does not modify spin-orbit coupling significantly (a few matrix elements are presented on ESI† Table S1). Therefore, from the spin-orbit coupling matrix elements, it is possible to conclude that there is no significant heavy-atom or symmetry related effect on the coupling between states, with the most probable pathway of intersystem crossing for corrole **2** being the S_1-T_1 transition.

3.5. Aggregation study by UV–vis spectroscopy

In a recent publication, tetrapyrrolic macrocyles with bulky moieties in a perpendicular orientation to the core structure are prevented from π-stacking interactions, therefore avoiding aggregation in solution [39]. To evaluate the aggregation behavior of corrole **2** in solution, we studied this phenomenon by UV–vis analysis in DCM. We observed that there was not a significant shift at the maximum absorbance wavelengths. A linear increase was observed in the absorption spectrum as a function of the concentration variation from 0.5–12 μM. In addition, new absorption band on the UV–vis region. Both observations indicate that aggregation is not present (ESI†, Fig. S10).

3.6. Singlet oxygen ($^1O_2$) quantum yield and photostability of corrole 2

The success of PDT depends on the capacity of molecules to generate cytotoxic singlet oxygen, which causes oxidative stress and membrane damage in the treated cells [40]. Therefore, the photodynamic activity of corrole **2** was indirectly evaluated for its possible use in photodynamic application. The ability of corrole **2** to produce $^1O_2$ was monitored using 1,3-diphenylisobenzofuran (DPBF) in aprotic solvent (DMSO) [41]. The DPBF method has been widely used to provide a quantitative analysis of singlet oxygen production since the reaction product (1,2-dibenzoylbenzene) does not absorb visible light. It is a popular measurement procedure because of its simplicity in evaluating $^1O_2$ generated by Type II photo processes [42]. In this procedure, changes on the DPBF absorbance are directly related to the amount of $^1O_2$ generated. Several research groups have suggested that Type II reactions are dominating in PDT, while Type I reaction occurs only when the cells are not well oxygenated, as under conditions of hypoxia or anoxia [43]. Fig. 6 shows the decrease in the DPBF absorbance, monitored at 415 nm during irradiation with a 660 nm diode laser, for corrole **2** in DMSO solution.

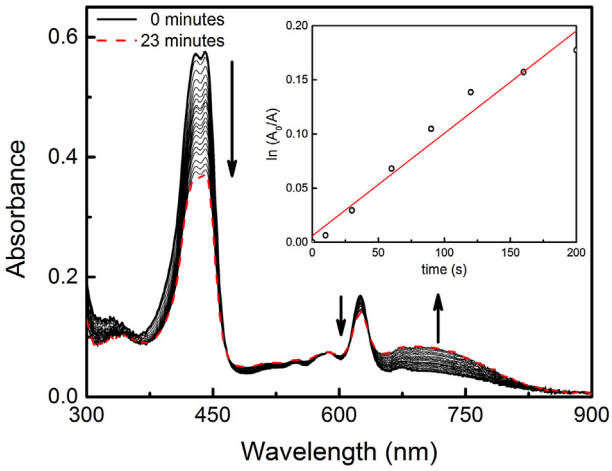

Fig. 6. Photodegradation of DPBF by irradiation with diode laser (660 nm) in the presence of corrole **2**. The inset shows the first order kinetic profile.

The most important parameter when evaluating the photodynamic activity of a photosensitizer is the singlet oxygen quantum yields (Φ_Δ) [44]. Φ_Δ is the ratio of the number of $^1O_2$ molecules procedure to the number of photons absorbed by photosensitizer. Therefore, it is a measure of the ability of the photosensitizer to generate cytotoxic singlet oxygen that destroys biomolecules. The value of Φ_Δ obtained of corrole **2** was 0.47, which is slightly lower than ZnPc, the standard samples used here ($\Phi_{Dstd} = 0.67$), but still displays good ability to generate singlet oxygen. The ability to generate $^1O_2$ of corrole **2** after being exposed to light and oxygen allowed us to envisage them as a potential photocleavage agent. The value of the singlet oxygen quantum yield of about 47% is close to the triplet quantum yield formation (51%) measured with PTF indicating that $^1O_2$ generated is proportional to the molecules in the triplet state.

Efficient photosensitizers must be stable when exposed to light for long periods of time. Thus, photo-bleaching evaluation is an important parameter for the study of photo-degradation of tetrapyrrolic macrocycles after irradiation with light, in which singlet oxygen reacts with the photosensitizer promoting its own degradation [45]. From the small changes on the absorbance spectrum as a function of the time, it was confirmed by corrole **2** presents a good stability when irradiated with a 100 mW diode laser with at 660 nm during 30 min (see ESI†, Fig. S11).

3.7. Electrochemistry and spectroelectrochemical analysis of corrole 2

The electroactive free-base corrole **2** (**H_3Cor**) showed irreversible and *quasi*-reversible electron transfer processes between −1.0 and +2.4 V *versus* SHE in CH_2Cl_2 at 0.1 V/s as seen in the cyclic voltammogram of Fig. 7. The assignment of the electrogenerated species was carried out by comparison with the electrochemistry of corroles containg *meso*-substituents [46], which showed similar behavior.

The electro-oxidation of corrole **2** (**H_3Cor**) at a Au electrode exhibited a complex redox pattern with peak potentials for the anodic scan at +0.50 V, +0.98 V, +1.26 V, +1.67 V and +2.10 V (Fig. 7). The peak at +0.50 V was seen only after the first anodic scan, and it

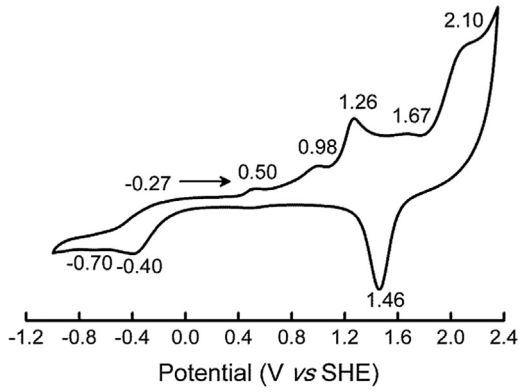

Fig. 7. Cyclic voltammogram of corrole **2** (**H_3Cor**) in dichloromethane containing 0.1 mol/L $TBAPF_6$, as support electrolyte, using a scan rate of 100 mV/s.

is related with the reduction process at −0.40 V, which will be discussed latter. The oxidation of corrole **2** (**H_3Cor**) at +0.98 V was assigned to the formation of the π-cation radical **$[H_3Cor]^+$**, which partially reacts with the neutral **H_3Cor** molecules from the bulk to give radical species **$[H_2Cor]$** and cation species **$[H_4Cor]^+$**. The species **$[H_2Cor]$**, **$[H_3Cor]^+$** and **$[H_4Cor]^+$** are further oxidized at +1.26 V, +1.67 V and +2.10 V respectively, generating cation and dications **$[H_2Cor]^+$**, **$[H_3Cor]^{2+}$** and **$[H_4Cor]^{2+}$**, see Scheme 2. There is a close correspondence of these values with those found for $H_3[((CF_3)_2Ph)_3Cor]$ in PhCN at +0.94 V, +1.25 and +1.63 V, although the potential at +1.63 V was not assigned in that study by Shen et al. [46].

The UV–vis spectral changes observed during the electro-oxidation of corrole **2** (**H_3Cor**) were followed by thin-layer spectroelectrochemistry and are shown in Fig. 8a and b. The free-base corrole **2** (**H_3Cor**) exhibits an UV band at 303 nm, a Soret band at 427 nm and visible bands at 567, 611 and 658 nm, respectively. Bands at 220 and 250 nm continuously gain intensity as the oxidation proceeds. The intensities of the π-π* transition at 303 nm and the Soret band decrease as a shoulder emerges at 450 nm. In the visible spectrum, the band at 658 nm also losses intensity relative to the new band at 590 nm. Kadish and co-workers reported the electrochemical characterization of alkyl- and aryl-substituted cobalt(III) corroles and observed four macrocycle-centered oxidations processes in CH_2Cl_2 with $E_{1/2}$ values in the range +0.69 to +1.50 *versus* SHE. The metal-centered processes were seen close to 0.0 V [47].

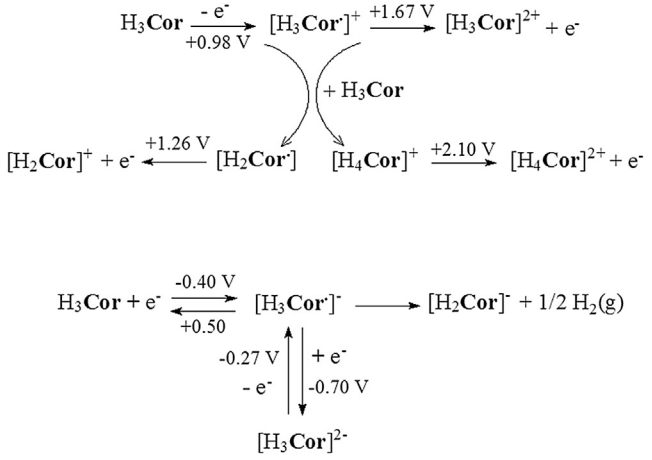

Scheme 2. Proposed redox behavior of corrole **2** (**H_3Cor**).

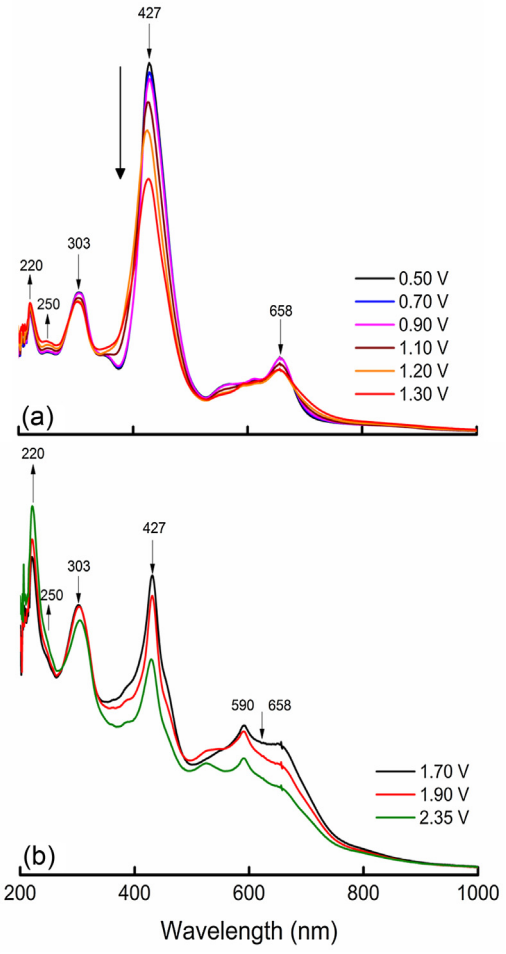

Fig. 8. Thin-layer UV–vis spectra changes during oxidation of corrole **2** (**H_3Cor**), (a) +0.50 to +1.30 V and (b) +1.70 to +2.35 V, using I = 0.10 mol/L $TBAPF_6$ in CH_2Cl_2. Potentials in Volt *versus* SHE.

The first reduction at −0.40 V is assigned to the formation of the π-anion radical **$[H_3Cor]^-$** through the irreversible monoeletronic process **$H_3Cor + e^- \rightarrow [H_3Cor]^-$**. This assignment is supported by changes observed in the thin-layer UV–vis spectra along with the electroreduction shown in Fig. 9. The spectral changes along with the controlled-potential reduction reveal that the Soret band intensity significantly diminishes and one the new spectrum shows a visible band at 620 nm.

The electrogenerated **$[H_3Cor]^-$** species most likely accepts a second electron at −0.70 V, in a low current intensity process, to give **$[H_3Cor]^{2-}$** species. The low current intensity is attributed to the slow decomposition of the **$[H_3Cor]^-$** species according to the reaction: **$[H_3Cor]^- \rightarrow [H_2Cor]^- + 1/2H_{2(g)}$**, as observed for related *meso*-substituted corroles [46,47], which also showed analogous UV–vis spectral patterns and irreversible reductions in the cyclic voltammetry measurements with reduction peak potentials at −0.79 V and −1.16 V *versus* SHE in benzonitrile solutions. The oxidation processes at −0.27 V and +0.503 V are coupled to the reduction peaks at −0.40 V and −0.70 V and are due to the following reactions: **$[H_3Cor]^{2-} \rightarrow [H_3Cor]^- + e^-$** and **$[H_3Cor]^- \rightarrow H_3Cor + e^-$**, regenerating the free-base corrole **2**. Finally, the peak at +0.96 V concentrates the major reduction processes in regenerating corrole **2** (**H_3Cor**), given that the charge number is 3.2×10^{-5} C, a figure close to the sum of the charge of the oxidations between +0.98 and +2.10 V (which is 2.0×10^{-5} C). A series of cobalt(III)-corrole complexes earlier reported [47] also showed two major

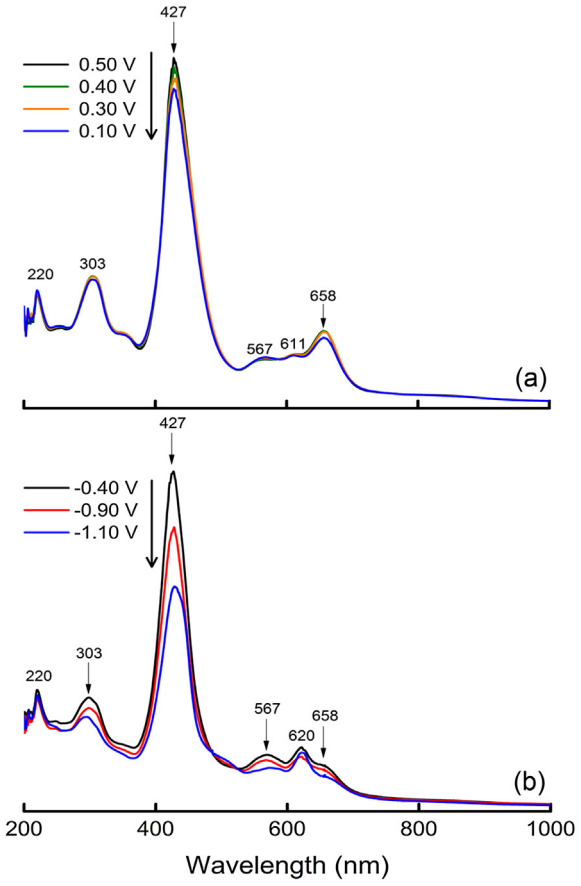

Fig. 9. Thin-layer UV–vis spectra changes during reduction of corrole **2** (**H_3Cor**), (a) +0.50 to +0.10 V and (b) −0.40 to −1.10 V, using I = 0.10 mol/L $TBAPF_6$ in CH_2Cl_2. Potentials in Volt *versus* SHE.

reductions in dichromethane between +0.09 and −1.46 V *versus* SHE.

4. Conclusion

In this work, we investigated and interpreted the excited state kinetics of corrole **2** dissolved in DCM. Singlet-triplet intersystem crossing was evaluated by time resolved fluorescence and pulse train fluorescence techniques. Our results demonstrated that the corrole **2** presents a considerable high triplet state formation, with about 51% quantum yields. This was obtained by modeling the suppression of the fluorescence signal employing a rate equations approach. We also determined the fluorescence and internal conversion quantum yields and observed that the main mechanisms responsible for the deactivation of the first singlet excited state are mediated by ISC and IC, both with almost the same probability. The singlet oxygen quantum yields of about 47% confirmed the high triplet state rate of formation for corrole **2**. Additionally, quantum chemistry calculations demonstrated that the most probable intersystem crossing pathway takes place through S_1-T_1, corroborating our rate equation model and that there is no significant heavy-atom or symmetry related effect on the coupling between the states.

Acknowledgements

Thanks are due to the CNPq, CAPES, FAPESP and INCT Catálise for researchers funding. R.C. Pivetta and B. L. Auras also thank CAPES and CNPq for their IC and master grants.

Appendix A. Supplementary data

Supplementary data associated with this article can be found, in the online version, at http://dx.doi.org/10.1016/j.jphotochem.2016.09.008.

References

[1] J.F.B. Barata, C.I.M. Santos, M.G.P.M.S. Neves, M.A.F. Faustino, J.A.S. Cavaleiro, Functionalization of corroles, Top. Heterocycl. Chem. 33 (2014) 79–142.
[2] A.W. Johnson, I.T. Kay, Corroles part I – synthesis, J. Chem. Soc. (1965) 1620–1629.
[3] Z. Gross, N. Galili, I. Saltsman, The first direct synthesis of corroles from pyrrole, Angew. Chem. Int. Ed. 38 (1999) 1427–1429.
[4] (a) B. Ventura, A.D. Esposti, B. Koszarna, D.T. Gryko, L. Flamigni, Photophysical characterization of free-base corroles, promising chromophores for light energy conversion and singlet oxygen generation, New J. Chem. 29 (2005) 1559–1566;
(b) B. Bursa, D. Wróbel, B. Barszcz, M. Kotkowiak, O. Vakuliuk, D.T. Gryko, Kolanowski Ł, M. Baraniak, G. Lota, The impact of solvents on the singlet and triplet states of selected fluorine corroles ?absorption, fluorescence, and optoacoustic studies, Phys. Chem. Chem. Phys. 18 (2016) 7216–7228.
[5] K.P. Butin, E.K. Beloglazkina, N.V. Zyk, Metal complexes with non-innocent ligands, Russ. Chem. Rev. 74 (2005) 531–553.
[6] Z. Gross, H.B. Gray, How do corroles stabilize high valent metals, Comments Inorg. Chem. 27 (2006) 61–72.
[7] B.J. Brennan, Y.C. Lam, P.M. Kim, X. Zhang, G.W. Brudvig, Photoelectrochemical cells utilizing tunable corroles, ACS Appl. Mater. Int. 7 (2015) 16124–16130.
[8] Y. Gao, J. Liu, M. Wang, Y. Na, B. Åkermark, L. Sun, Synthesis and characterization of manganese and copper corrole xanthene complexes as catalysts for water oxidation, Tetrahedron 63 (2007) 1987–1994.
[9] (a) A.S. Pereira, J.F.B. Barata, V.I.R.C. Vaz Serra, S. Pereira, T. Trindade, A green method for the preparation of fluorescent hybrid structures of gold and corrole, J. Nanopart. Res. 17 (2015) 392–402;
(b) C.I.M. Santos, E. Oliveira, J.F.B. Barata, M.A.F. Faustino, J.A.S. Cavaleiro, M.G.P. M.S. Neves, C. Lodeiro, Corroles as anion chemosensors: exploiting their fluorescence behaviour from solution to solid-supported devices, J. Mater. Chem. 22 (2012) 13811–13819.
[10] (a) H. Agadjanian, J. Ma, A. Rentsendorj, V. Valluripalli, J.Y. Hwang, A. Mahammed, D.L. Farkas, L.K. Medina-Kauwe, Tumor detection and elimination by a targeted gallium corrole, Proc. Natl. Acad. Sci. U. S. A. 106 (2009) 6105–6110;
(b) C.M. Blumenfeld, B.F. Sadtler, G.E. Fernandez, L. Dara, C. Nguyen, F. Alonso-Valenteen, L.K. Medina-Kauwe, R.A. Moats, N.S. Lewis, R.H. Grubbs, H.B. Gray, K. Sorasaenee, Cellular uptake and cytotoxicity of a near-IR fluorescent corrole–TiO_2 nanoconjugate, J. Inorg. Biochem. 140 (2014) 39–44.
[11] J.F.B. Barata, M.G.P.M.S. Neves, A.C. Tomé, M.A.F. Faustino, A.M.S. Silva, J.A.S. Cavaleiro, How light affects 5,10,15-tris(pentafluorophenyl)corrole, Tetrahedron Lett. 51 (2010) 1537–1540.
[12] (a) For functionalization methods see:, L.S.H.P. Vale, J.F.B. Barata, C.I.M. Santos, M.G.P.M.S. Neves, M.A.F. Faustino, A.C. Tomé, A.M.S. Silva, F.A.A. Paz, J.A.S. Cavaleiro, Corroles in 1,3-dipolar cycloaddition reactions, J. Porphyrins Phthalocyanines 13 (2009) 358–368;
(b) G. Pomarico, M. Stefanelli, S. Nardis, S. Lentini, D.O. Cicero, G.T. McCandless, K.M. Smith, R. Paolesse, Synthesis and functionalization of β-alkyl-*meso*-triarylcorroles, J. Porphyrins Phthalocyanines 19 (2015) 865–873;
(c) M. Stefanelli, S. Nardis, L. Tortora, F.R. Fronczek, K.M. Smith, S. Licoccia, R. Paolesse, Nitration of iron corrolates: further evidence for non-innocence of the corrole ligand, Chem. Commun. 47 (2011) 4255–4257;
(d) I. Saltsman, A. Mahammed, I. Goldberg, E. Tkachenko, M. Botoshansky, Z. Gross, Selective Substitution of Corroles: Nitration, Hydroformylation, and Chlorosulfonation, J. Am. Chem. Soc. 124 (2002) 7411–7420;
(e) T.H. Ngo, F. Puntoriero, F. Nastasi, K. Robeyns, L. Van Meervelt, S. Campagna, W. Dehaen, W. Maes, Synthetic, structural, and photophysical exploration of meso-pyrimidinyl-substituted AB_2-corroles, Chem. Eur. J. 16 (2010) 5691–5705.
[13] (a) T.A.F. Cardote, J.F.B. Barata, M.A.F. Faustino, A. Preuß, M.G.P.M.S. Neves, J.A.S. Cavaleiro, C.I.V. Ramos, M.G.O. Santana-Marques, B. Röder, Pentafluorophenylcorrole–D-galactose conjugates, Tetrahedron Lett. 53 (2012) 6388–6393;
(b) F. Faschinger, S. Aichhorn, M. Himmelsbach, W. Schoefberger, Bismuth A_3-corroles: useful precursors for the development of meso-substituted free-base corroles, Synthesis 46 (2014) 3085–3096.
[14] (a) H. Ma, M. Zhang, D. Zhang, R. Huang, Y. Zhao, H. Yang, Y. Liu, X. Weng, Y. Zhou, M. Deng, L. Xu, X. Zhou, Pyridyl-substituted corrole isomers: synthesis and their regulation to G-quadruplex structures, Chem. Asian J. 5 (2010) 114–122;
(b) I. Saltsman, M. Botoshansky, Z. Gross, Facile synthesis of ortho-pyridyl-substituted corroles and molecular structures of analogous porphyrins, Tetrahedron Lett. 49 (2008) 4163–4166.
[15] Y. Gao, J. Liu, W. Jiang, M. Xia, W. Zhang, M. Li, B. Åkermark, L. Sun, Synthesis and photophysical and electrochemical properties of a binuclear Ru(bpy)$_3$-Cu (III) corrole complex, J. Porphyrins Phthalocyanines 11 (2007) 463–469.

[16] (a) D.T. Gryko, B. Koszarna, Refined methods for the synthesis of meso-substituted A_3- and trans-A_2B-corroles, Org. Biomol. Chem. 1 (2003) 350–357;
(b) B. Koszarna, D.T. Gryko, Efficient synthesis of *meso*-substituted corroles in a H_2O-MeOH mixture, J. Org. Chem. 71 (2006) 3707–3717;
(c) D.T. Gryko, Recent advances in the synthesis of corroles and core-modified corroles, Eur. J. Org. Chem. 2002 (2002) 1735–1743;
(d) J.K. Laha, S. Dhanalekshmi, M. Taniguchi, A. Ambroise, J.S.A. Lindsey, Scalable synthesis of *meso*-substituted dipyrromethanes, Org. Process Res. Dev. 7 (2003) 799–812.
[17] (a) L. De Boni, P.L. Franzen, P.J. Gonçalves, I.E. Borissevitch, L. Misoguti, C.R. Mendonça, S.C. Zílio, Pulse train fluorescence technique for measuring triplet state dynamics, Opt. Express 19 (2011) 10813–10823;
(b) T.G.B. de Souza, M.G. Vivas, C.R. Mendonça, S. Plunkett, M.A. Filatov, M.O. Senge, L. De Boni, Studying the intersystem crossing rate and triplet quantum yield of meso-substituted porphyrins by means of pulse train fluorescence technique, J. Porphyrins Phthalocyanines 20 (2016) 282–291.
[18] F. Neese, The ORCA program system, Comput. Mol. Sci. 2 (2012) 73–78 Wiley Int. Rev..
[19] J.P. Perdew, K. Burke, M. Ernzerhof, Generalized gradient approximation made simple, Phys. Rev. Lett. 77 (1996) 3865.
[20] F. Weigend, R. Ahlrichs, Balanced basis sets of split valence, triple zeta valence and quadruple zeta valence quality for H to Rn: design and assessment of accuracy, Phys. Chem. Chem. Phys. 7 (2005) 3297–3305.
[21] S. Sinnecker, A. Rajendran, A. Klamt, M. Diedenhofen, F. Neese, Calculation of solvent shifts on electronic g-tensors with the conductor-Like screening model (COSMO) and its self-consistent generalization to real solvents (Direct COSMO-RS), J. Phys. Chem. A 110 (2006) 2235–2245.
[22] S. Grimme, S. Ehrlich, L. Goerigk, Effect of the damping function in dispersion corrected density functional theory, J. Comput. Chem. 32 (2011) 1456–1465.
[23] F. Neese, G. Olbrich, Efficient use of the resolution of the identity approximation in time-dependent density functional calculations with hybrid density functional, Chem. Phys. Lett. 362 (2002) 170–178.
[24] (a) C. Hadjur, N. Lange, J. Rebstein, P. Monnier, H. Van den Bergh, G. Wagnières, Spectroscopic studies of photobleaching and photoproduct formation of meta (tetrahydroxyphenyl)chlorin (m-THPC) used in photodynamic therapy. The production of singlet oxygen by m-THPC, J. Photochem. Photobiol. B 45 (1998) 170–178;
(b) M.P. Romero, N.R.S. Gobo, K.T. de Oliveira, Y. Iamamoto, O.A. Serra, S.R.W. Louro, Photophysical properties and photodynamic activity of a novel menthol–zinc phthalocyanine conjugate incorporated in micelles, J. Photochem. Photobiol. A 253 (2013) 22–29.
[25] (a) M. Durmus, T. Nyokong, Synthesis, photophysical and photochemical studies of new water-soluble indium(III) phthalocyanines, Photochem. Photobiol. Sci. 6 (2007) 659–668;
(b) T.H. de Souza, F.I. Ziembowicz, D.F. Müller, S.C. Lauermann, C.L. Kloster, R.C. V. Santos, L.Q.S. Lopes, A.F. Ourique, G. Machado, M.A. Villetti, Evaluation of photodynamic activity, photostability and in vitro drug release of zinc phthalocyanine-loaded nanocapsules, Eur. J. Pharm. Sci. 83 (2016) 88–98.
[26] G. Braga, J.L. Aparicio, B.H. Vilsinski, A.L. Tessaro, A.P. Gerola, N. Hioka, W. Caetano, Self-aggregation of 5,10,15,20-tetrakis(4-methoxyphenyl)porphyrin (tmpp): spectroscopic studies and multivariate analyzes, Quim. Nova 37 (2014) 648–652.
[27] C. Busche, P. Comba, A. Mayboroda, H. Wadepohl, Novel Ru^{II} complexes with bispidine-based bridging ligands: luminescence sensing and photocatalytic properties, Eur. J. Inorg. Chem. 2010 (2010) 1295–1302.
[28] D.F. Eaton, Reference materials for fluorescence measurement, Pure Appl. Chem. 60 (1988) 1107–1114.
[29] A.M. Brouwer, Standards for photoluminescence quantum yield measurements in solution, Pure Appl. Chem. 83 (2011) 2213–2228.
[30] L. De Boni, C. Toro, F.E. Hernandez, Excited state absorption study in hematoporphyrin IX, J. Fluoresc. 20 (2010) 197–202.
[31] T.M. Aminabhavi, V.B. Patil, Density, Viscosity, Refractive Index and Speed of Sound in Binary Mixtures of Ethenylbenzene with *NN*-Dimethylacetamide, Tetrahydrofuran, *NN*-Dimethylformamide, 1,4-Dioxane, Dimethyl Sulfoxide, Chloroform, Bromoform, and 1-Chloronaphthalene in the Temperature Interval (298. 15–308.15 K Department of Chemistry, 43, Karnatak University, Dharwad, 1998, pp. 497.
[32] T. Ding, E.A. Alemán, D.A. Modarelli, C.J. Ziegler, Photophysical properties of a series of free-base corroles, J. Phys. Chem. A 109 (2005) 7411–7417.
[33] (a) W. Shao, H. Wang, S. He, L. Shi, K. Peng, Y. Lin, L. Zhang, L. Ji, H. Liu, Photophysical properties and singlet oxygen generation of three sets of halogenated corroles, J. Phys. Chem. B 116 (2012) 14228–14234;
(b) L. Zhang, Z.-Y. Liu, X. Zhan, L.-L. Wang, H. Wang, H.-Y. Liu, Photophysical properties of electron-deficient free-base corroles bearing *meso*-fluorophenyl substituents, Photochem. Photobiol. Sci. 14 (2015) 562–953.
[34] L. De Boni, C.J.P. Monteiro, C.R. Mendonça, S.C. Zílio, P.J. Gonçalves, Influence of halogen atoms and protonation on the photophysical properties of sulfonated porphyrins, Chem. Phys. Lett. 633 (2015) 146–151.
[35] L. Shi, H.Y. Liu, H. Shen, J. Hu, G.L. Zhang, H. Wang, L.N. Ji, C.K. Chang, H.F. Jiang, Fluorescence properties of halogenated mono-hydroxyl corroles: the heavy-atom effects, J. Porphyrins Phthalocyanines 13 (2009) 1221–1226.
[36] J. Capar, J. Conradie, C.M. Beavers, A. Ghosh, Molecular structures of free-base corroles: nonplanarity, chirality, and enantiomerization, J. Phys. Chem. A 119 (2015) 3452–3457.
[37] W. Beenken, M. Presselt, T.H. Ngo, W. Dehaen, W. Maes, M. Kruk, Molecular structures and absorption spectra assignment of corrole NH tautomers, J. Phys. Chem. A 118 (2014) 862–871.
[38] F. Neese, Efficient and accurate approximations to the molecular spin-orbit coupling operator and their use in molecular g-tensor calculations, J. Chem. Phys. 122 (2005) 034107–034120.
[39] (a) M. Stefanelli, D. Monti, M. Venanzi, R. Paolesse, Kinetic and spectroscopic studies on the self-aggregation of a meso-substituted amphiphilic corrole derivative, New J. Chem. 31 (2007) 1722–1725;
(b) A.F. Uchoa, K.T. de Oliveira, M.S. Baptista, A.J. Bortoluzzi, Y. Iamamoto, O.A. Serra, Chlorin Photosensitizers Sterically Designed To Prevent Self-Aggregation, J. Org. Chem. 76 (2011) 8824–8832;
(c) F.A.B. dos Santos, A.F. Uchoa, M.S. Baptista, Y. Iamamoto, O.A. Serra, T.J. Brocksom, K.T. de Oliveira, Synthesis of functionalized chlorins sterically-prevented from self-aggregation, Dyes Pigm. 99 (2013) 402–411;
(d) J.M. de Souza, F.F. de Assis, C.M.B. Carvalho, J.A.S. Cavaleiro, T.J. Brocksom, K. T. de Oliveira, Synthesis of non-aggregating chlorins and isobacteriochlorins from meso-tetrakis(pentafluorophenyl)porphyrin: a study using 1 3-dipolar cycloadditions under mild conditions, Tetrahedron Lett. 55 (2014) 1491–1495.
[40] S.K. Sharma, L.Y. Chiang, M.R. Hamblin, Photodynamic therapy with fullerenes in vivo: reality or a dream, Nanomedicine 6 (2011) 1813–1825.
[41] J.F.B. Barata, A.L. Daniel-da-Silva, M.G.P.M.S. Neves, J.A.S. Cavaleiro, T. Trindade, Corrole-silica hybrid particles: synthesis and effects on singlet oxygen generation, RSC Adv. 3 (2013) 274–280.
[42] X.F. Zhang, X. Li, The photostability and fluorescence properties of diphenylisobenzofuran, J. Lumin. 131 (2011) 2263–2266.
[43] M. Ethirajan, Y. Chen, P. Joshi, R.K. Pandey, The role of porphyrin chemistry in tumor imaging and photodynamic therapy, Chem. Soc. Rev. 40 (2011) 340–362.
[44] A. Preuß, I. Saltsman, A. Mahammed, M. Pfitzner, I. Goldberg, Z. Gross, B. Röder, Photodynamic inactivation of mold fungi spores by newly developed charged corroles, J. Photochem. Photobiol. B 133 (2014) 39–46.
[45] (a) P.F.C. Menezes, C.A.S. Melo, V.S. Bagnato, H. Imasato, J.R. Perussi, Dark cytotoxicity of the photoproducts of the photosensitizer Photogem after photobleaching induced by a laser, Laser Phys. 15 (2005) 435–442;
(b) P. Kluson, M. Drobek, A. Kalaji, S. Zarubova, J. Krysa, J. Rakusan, Singlet oxygen photogeneration efficiencies of a series of phthalocyanines in well-defined spectral regions, J. Photochem. Photobiol. A 199 (2008) 267–273.
[46] J. Shen, J. Shao, Z. Ou, E. Wenbo, B. Koszarna, D.T. Gryko, K.M. Kadish, Electrochemistry and spectroelectrochemistry of *meso*-substituted free-base corroles in nonaqueous media: reactions of $(Cor)H_3$, $[(Cor)H_4]^+$, and $[(Cor)H_2]^-$, Inorg. Chem. 45 (2006) 2251–2265.
[47] J. Shao, Z. Ou, C.P. Gros, F. Bolze, J.-M. Barbe, R. Guilard, Alkyl- and aryl-substituted corroles. 4. Solvent effects on the electrochemical and spectral properties of cobalt corroles, Inorg. Chem. 42 (2003) 4062–4070.